Optical Control of Reconfigurable Antennas and Application to a Novel Pattern-Reconfigurable Planar Design

Damiano Patron, *Student Member, IEEE*, Afshin S. Daryoush, *Fellow, IEEE*, and Kapil R. Dandekar, *Senior Member, IEEE*

(Invited Paper)

***Abstract*—This paper discusses techniques for optical control of reconfigurable antennas using commercially available devices. These techniques are applied to a pattern-reconfigurable planar antenna that integrates optical control circuitry to switch folded microstrip radiators arranged in each of the quadrants. By switching between the microstrip elements, the designed antenna can generate a single omnidirectional or four directional patterns, maintaining good impedance matching within the 2.4 GHz WiFi band. We investigated two possible strategies for optical control: 1) p-i-n photodectors based switching, and 2) phototransistor controlled RF p-i-n diodes switches. Extended numerical and experimental analysis was carried out for the latter technique, discussing advantages and limitations when employed as RF switch on reconfigurable antennas. Finally, measurements of input impedance and radiation patterns were collected to validate the proposed optically controlled antenna design and compared to standard electronic control.**

***Index Terms*—Antennas, optical switches, photodetectors, phototransistors, reconfigurable architectures.**

I. Introduction

OPTICALLY controlled reconfigurable antennas are a class of radiating elements that are able to change their radiation properties through optical activation of silicon switches or reactive elements. With respect to the conventional dc control of lumped components, the use of optically controlled devices is preferable because they eliminate the need for metallic wires that may interfere with the antennas' radiation characteristics [1]. Additionally, while the switching speed of dc-controlled lumped elements is typically limited by external control circuitry, the use of photonic components is significantly faster. Other important aspects, such as the thermal and electrical isolation from the control circuitry make the photonic switching technique a very attractive solution relative to conventional dc control of lumped elements.

Generally speaking, reconfigurable antennas can be divided into two main categories: frequency-reconfigurable antennas which are able to adapt their resonant frequency based on the desired operational frequency [2], and, pattern-reconfigurable antennas which can change their radiation pattern or polarization in order to enhance the capacity of the wireless channel [3]. Such reconfigurability is typically provided by changing the current distribution on the metallic elements through switching [4] or reactive components [5], such as p-i-n diodes or varactor diodes.

However, the dc control of reconfigurable antennas often requires additional metallic microstrip or wired biasing lines, which add more complexity and may interfere with the desired radiation pattern. In order to overcome this issue, several optically controlled reconfigurable antennas have been reported in the literature. In [6], [7], the authors propose a frequency-reconfigurable antenna designed using photoconductive switches. The laser light is coupled through an optical fiber that passes through the substrate by means of a proper fixture to illuminate the switches connected to the top layer metallic elements. A reconfigurable monopole antenna, presented in [8], employs photoconductive switches illuminated in free space to switch between metallic branches and thus change resonant frequency. In [9] the authors propose an optically reconfigurable dipole antenna which can vary frequency and radiation pattern by switching between short and long configurations of the conductive arms. However, in all of these designs, the authors use customized photoconductive switches that are not commercially available.

In this paper, we investigate two possible strategies for the optical control of reconfigurable antennas using commercially available devices:

1) p-i-n photodector with a pig-tailed optical fiber, where switching functions are accomplished using change in the intrinsic capacitance under reverse bias condition.
2) Switching control of RF p-i-n diodes accomplished through the optical illumination of a phototransistor, equipped with a proper biasing network.

Both switching strategies have been numerically and experimentally analyzed in order to evaluate their respective advantages and limitations.

Manuscript received January 1, 2014; revised March 16, 2014; accepted April 21, 2014. Date of publication April 30, 2014; date of current version September 1, 2014. This paper is based upon work supported by the National Science Foundation under Grants CNS-0916480 and CNS-1147838. A preliminary version of this paper appeared in the proceedings of the 2013 IEEE Microwave Photonics Conference.

The authors are with the Department of Electrical and Computer Engineering, Drexel University, Philadelphia, PA 19104 USA (e-mail: damiano.patron@drexel.edu; daryoush@coe.drexel.edu; dandekar@coe.drexel.edu).

Color versions of one or more of the figures in this paper are available online at http://ieeexplore.ieee.org.

Digital Object Identifier 10.1109/JLT.2014.2321406

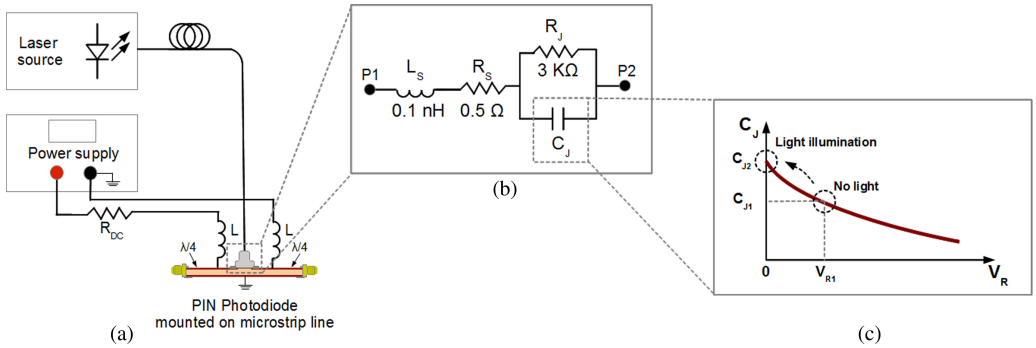

Fig. 1. (a) p-i-n Photodiode mounted on a proper microstrip line for S-parameter measurements. Detail of the resistive element $R_{\rm DC}$ to accomplish voltage drop under photocurrent generation. (b) p-i-n Photodiode equivalent model. (c) Plot of capacitance C_J versus reverse voltage V_R and sketch of the bias point change due to voltage drops across the series resistance $R_{\rm DC}$, when photocurrent is generated under light illumination.

Next, the design of an optically controlled reconfigurable planar antenna is presented. This antenna is able to generate a single omnidirectional or four directional beams by switching between microstrip elements. The design is tuned to operate within the 2.4 GHz WiFi band and exhibit good impedance matching under optical control in all of the configurations. Along with the benefits of fully optical control, the proposed antenna allows for the generation of omnidirectional and directional beams in a single compact design. This beam adaptation functionality provides a valuable degree of freedom to wireless links operating in challenging multi-client and multipath scenarios [10], [11].

The paper is organized as follows: Section II presents two optical switching techniques, focusing on the experimental analysis of the best strategy. Then, Section III describes the proposed antenna design along with the optical control circuitry, impedance and radiation characteristic measurements. Finally, conclusions are drawn in Section IV.

II. Optical Switching Techniques

Single-pole single-throw (SPST) switches have found wide usage in RF applications such as microwave circuits and reconfigurable antennas. Their impedance, measured through S_{12} or S_{21} scattering parameters, can be controlled by a dc excitation, and switch between high isolation (OFF mode) and low insertion loss (ON mode) states. High isolation can be established when the impedance is such that more than 90% of the RF power is being blocked (i.e., S_{21} below -10 dB). Conversely, low insertion loss is achieved when more than 90% of the energy is flowing through the device (i.e., S_{21} between 0 and -0.5 dB). The aim of this section is to discuss the best strategy to realize optically-controlled SPST using commercially available devices. We describe two possible solutions, focusing on a phototransistor topology which showed proper isolation and insertion loss for use in reconfigurable antennas.

A. Photocurrent Generation Through p-i-n Photodetector

The first device considered as a potential switching element, is a commercial p-i-n photodiode [23] with two-port small lids to provide photodiode operation through collection of photocurrent flow. In order to evaluate the p-i-n photodiode RF switching performance, we employed a change in operation point taking advantage of the variation in the junction capacitance C_J under different levels of 1550 nm laser illumination. As depicted in Fig. 1(a), the device was mounted on two λ/4 microstrip lines connected to SMA ports for scattering parameter (S-Parameter) characterization by vector network analyzer. Due to poor performance under fixed reverse bias voltage V_R, we employed larger photovoltaic changes by adding a resistor $R_{\rm DC}$ in series to the dc bias line. As a result, a significant change in the bias voltage of the photodiode is accomplished due to the generated photocurrent under optical illumination, Fig. 1(c). A detailed description of the measured and simulated performance has been presented in [12]. In summary, the measurements conducted under different optical power have demonstrated a good insertion loss of 0.6 dB but poor isolation of only 3.3 dB. Additional simulations of the lumped equivalent model in Fig. 1(b) show that for capacitance C_J between 0.1 and 1.5 pF the p-i-n photodiode may guarantee isolation of over 10 dB and insertion loss of under 0.5 dB to be used as RF switch in reconfigurable antennas within the microwave region from 2 to 3 GHz. Such a large change in capacitance could be accomplished using custom designed photodiodes with interesting photodetector structures [13], [14]. However, in the next section, we present an alternative method that we have analyzed to ensure good RF switching performance through optical control.

B. Phototransistor as Optical Control of RF p-i-n Diodes

The second proposed optical technique combines the benefit of using an electrical p-i-n diode specifically designed for RF switching, and a phototransistor for the optical control. For a p-i-n diode we selected the Skyworks SMP-1345. This 1.2 × 0.8 mm SMD package device has very low capacitance and is designed for high isolation and low insertion loss in wireless applications. As optical control, a silicon-based Everlight PT19–21B phototransistor was employed with a 20 mA collector current, which is sufficient for driving up to two p-i-n diodes in two forward biases. In this two-terminal phototransistor, the maximum collector-emitter voltage $V_{\rm CE}$ is 30V and saturation voltage $V_{CE(\rm sat)}$ is 0.4 V. This model has been preferred thanks to its small 1.2 × 0.8 mm SMD package as well as fast response time and high photo sensitivity. Generally speaking, the phototransistor is in essence a bipolar transistor having a transparent package so that light can reach the base-collector junction. The electrons generated by the incoming light are amplified by the

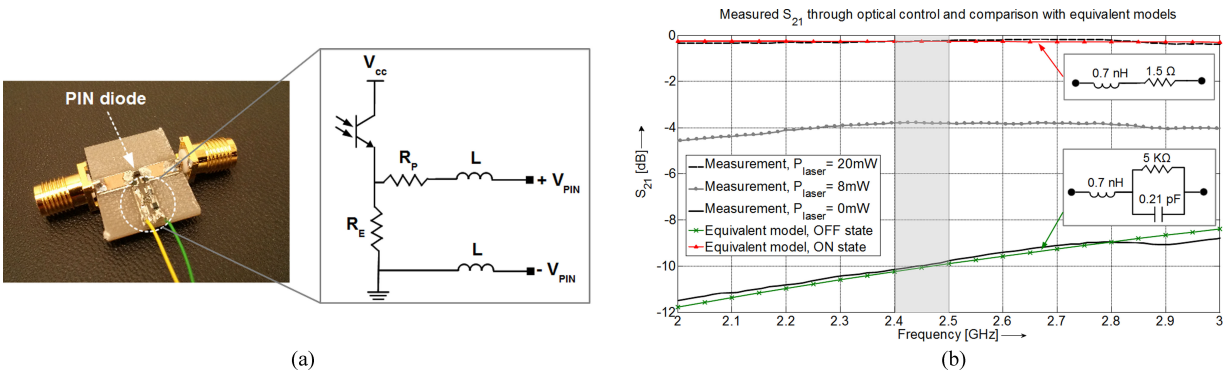

(a) (b)

Fig. 2. (a) p-i-n diode mounted on microstrip lines for S-parameter measurements and detail of the optical control circuitry. (b) S_{21} measurements of the p-i-n diode under different levels of $\lambda = 850$ nm laser illumination on the phototransistor. Lumped equivalent models of ON and OFF states are also shown.

TABLE I
PT19-21B PHOTOTRANSISTOR CHARACTERISTICS

Collector current I_C	20 mA
Wavelength of peak sensitivity	940 nm
Responsivity	0.9 A/W
Collector dark current	100 nA

transistor's current gain β, allowing for current to flow from the two poles of the device. The main characteristics of the selected phototransistor, reported in the component's datasheet [22], are summarized in Table I.

A picture of the p-i-n diode mounted on microstrip lines for S-parameter measurements is shown in Fig. 2(a), along with the schematic of the control circuitry is also depicted in this figure. When the phototransistor is not illuminated, the voltage across the p-i-n diode $(V_{\rm PIN})$ is equal to zero and thus the p-i-n diode is in a high isolation state (OFF). On the other hand, under optical illumination, a photocurrent flows between the collector and emitter poles of the phototransistor. A resistive network ($R_E = 10$ kΩ, $R_P = 470$ Ω) provides a proper voltage drop that is required for changing the bias condition of RF p-i-n diode, hence, enabling a required insertion reduction for switching from OFF to ON states of the RF p-i-n diode ($V_{\rm PIN} = 1$ V, $I = 10$ mA).

S-parameter measurements were carried out to analyze the p-i-n diode performance under different laser levels incident to the phototransistor. As a light source, we used a free space 850 nm laser (Vixar VCSEL), which corresponds to a responsivity of 0.9 A/W of the phototransistor. Similarly to the previous measurements, calibration of the vector network analyzer was made by de-embedding λ/4 microstrip lines used to solder the p-i-n diode. The measured S_{21} performance of this RF p-i-n diode is depicted in Fig. 2(b) under three different VCSEL optical powers. Under dark condition the isolation at 2.45 GHz is about 10 dB, whereas when the light incident to the phototransitor exceeds 8 mW, the generated photocurrent switches the p-i-n diode to conduction mode. However, the best value of insertion loss, $S_{21} = -0.3$ dB at 2.45 GHz, is achieved when the VCSEL is biased for free-space optical power of 20 mW. Note the level of light coupling to photo-transistor through its optical window is significantly less, as now an optical focusing mechanism is used in this topology. Through the use of a 2D micropositioner for *x*-*y* tilting, and an adjustable base for *z* axis, the laser source was aligned to the phototransistor's flat-top photosensitive area, achieving a light coupling sufficient to create a biasing current flowing of 10 mA.

The presence of lumped switching elements in reconfigurable antennas often requires additional control boards to boost the current from the general purpose input/output pins of the wireless radio platform. For comparison, a traditional MOSFET based topology would exploit the same circuit topology as in Fig. 2(a). However, the use of a 1 mm^2 two-terminal phototransistor instead of a conventional SOT-23 3.7 mm^2 3-terminal MOSFET, allows us to unobtrusively integrate the switching circuit in close proximity to the non-radiating area of the proposed antenna, eliminating the dc wires for gates control. We specifically selected small package SMD components, which occupy a total area of about 4 mm^2, maintaining full substrate robustness. Despite the fact that this technique involves the use of multiple components, the occupied area is comparable to the p-i-n photodiode discussed in Section II-A while resulting in a good, cost-effective solution.

Beyond the aforementioned promising performance in terms of isolation and insertion loss, this technique is also less affected by the noise in the laser source, as the RF impedance of the switching element is not directly related to the generated photocurrent. In other words, since we take advantage of the ON/OFF behavior of a phototransistor, small variations of light intensity around its high responsivity region do not lead to significant change in the relative RF insertion loss. In fact, at the responsivity region of 0.9 A/W, small variations in the order of 15–20% of the optical power lead to very limited changes in the forward current that flows through the p-i-n diode. As a result, the p-i-n diode series resistance does not change significantly and the insertion loss has been observed to sweep between $0.4 \leq S_{21} \leq 0.2$ dB.

The good performance demonstrated by this technique, allowed us to apply the optical switching circuitry to a planar reconfigurable antenna. The next section describes the implemented antenna design along with the integrated optical control layout. The whole radiating system is then validated with comprehensive input impedance and radiation pattern measurements.

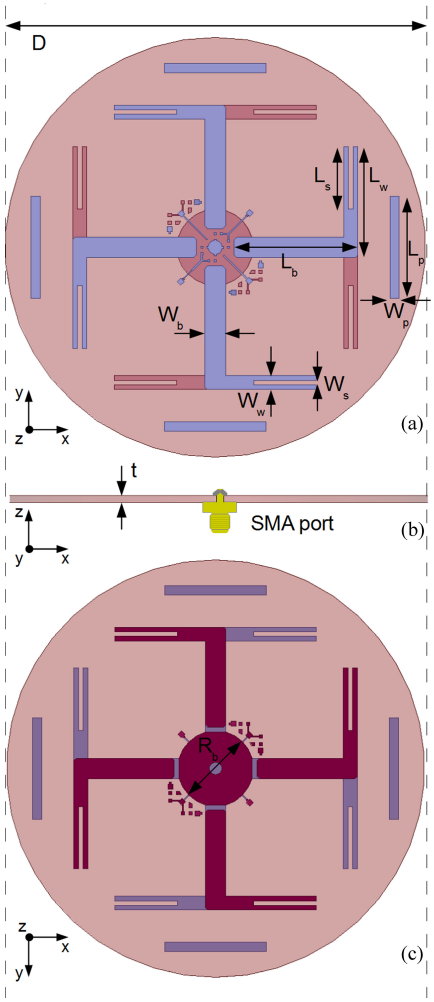

Fig. 3. 3D model of the proposed reconfigurable planar antenna. (a) Top layer view. (b) Horizontal profile with RF input port detail. (c) Bottom layer view. The small pads and lines visible on both layers constitute the arrangement for the SMD components population.

III. Antenna Design and Characterization

The proposed reconfigurable antenna was motivated by the need to generate omnidirectional and directional radiation patterns in a single planar design. For this purpose we have applied the concept of the Alford Loop Antenna [15], [16] and re-designed the metallic elements making the system a compact pattern-reconfigurable antenna.

The layout is made of four pairs of 90° microstrip elements arranged symmetrically between top and bottom layer of a standard FR-4 substrate, as shown in Fig. 3(a) and (c). Four additional microstrip parasitics in front of each pair are placed on the top layer to enhance directivity under directional beam operations. The antenna is fed by a coaxial SMA port connected to the bottom layer with ground, while the inner conductor is soldered on top through a via hole, Fig. 3(b). Pads and gaps on the top and bottom layer are designed to include the RF p-i-n diodes along with the optical control circuitry described in Section II-B and depicted in Fig. 4. Substrate details and antenna dimensions are listed in Table II.

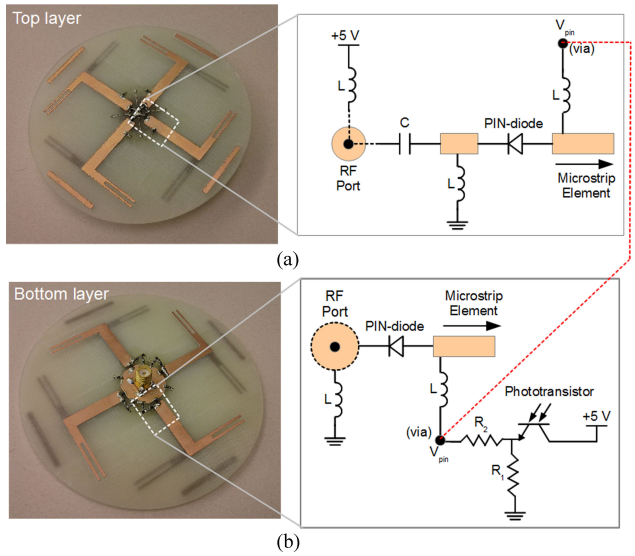

Fig. 4. Manufactured prototype and details of the optical switching circuitry for a pair of symmetric elements. (a) Top layer biasing circuitry. (b) Bottom layer optical and biasing circuitry. The voltage and current activated by the phototransistor, are shared between the two layers through a via hole (red dashed line).

TABLE II
Substrate Characteristics and Antenna Dimensions

Value	Description	Value	Description
t= 1.6 mm	Substrate thickness	W_w= 3.3 mm	Wing width
c= 0.035 mm	Copper thickness	L_w= 26.5 mm	Wing length
ε_r= 4.4	Dielectric constant	W_p= 2.2 mm	Parasitic width
D= 90 mm	Antenna diameter	L_p= 24.2 mm	Parasitic length
R_b= 18.2 mm	Bottom circle diameter	L_s= 14.9 mm	Slot length
W_b= 4.9 mm	Branch width	W_s= 1.1 mm	Slot width
L_b= 29.5 mm	Branch length		

To maintain purely optical control, the necessary bias voltage for the driving circuitry is provided by means of a bias-tee connected to the RF input port. As depicted in Fig. 4(a), the positive bias is extracted on the top layer from the RF inner conductor using a $L = 220$ nH RF-choke inductor and decoupled from the ground through a $C = 15$ pF dc-block capacitor. On the bottom layer, shown in Fig. 4(b), the phototransistor along with the resistive network $R_1 = 10$ KΩ and $R_2 = 200$ Ω create the necessary bias condition $V_{\rm PIN}$ to switch ON and OFF the p-i-n diodes on top and bottom layer.

The antenna layout was designed and tuned using the full-wave electromagnetic simulator Ansoft HFSS [24]. In order to perform more realistic simulations, lumped equivalent models of the p-i-n diode [25] have been extracted for the best fit with the measurements depicted in Fig. 2(b). The models where then loaded into the HFSS antenna design in the form of *RLC* lumped ports.

A. Modes of Operation

By switching between the pairs of microstrip elements, the antenna can generate a single omnidirectional or four distinct directional beams with 90° separation. Good impedance matching over the 2.4 GHz WiFi band for all the configurations is accomplished by tuning the diameters of the top and bottom layer circles as well as the slot length in each microstrip wing.

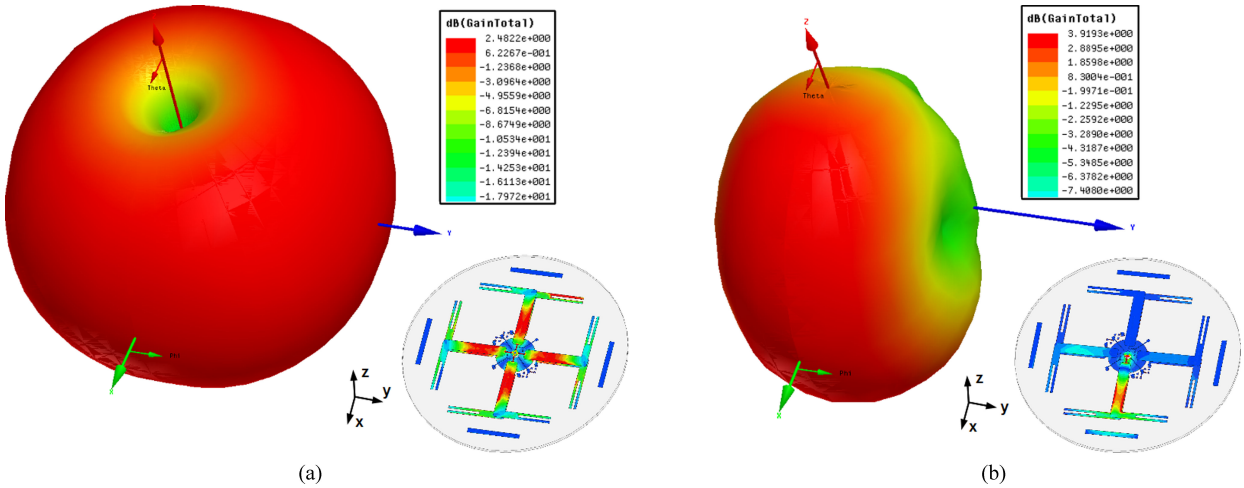

Fig. 5. (a) Omnidirectional mode, all microstrip elements activated and uniform current distribution. (b) Single directional mode, only the pair of elements directed in positive x direction are activated. The disabled pairs reflect the beam and enhance its directivity towards x direction.

For both modes of operation, the comparison between simulated and measured input impedance is shown in Fig. 6 and discussed in Section III-B. The next two sections describe the patterns characteristics, simulated with the software HFSS.

1) Omnidirectional Mode: A single omnidirectional radiation pattern is generated when all the microstrip elements are connected to the central RF port. In this state the currents distribution is uniform along the structure, radiating a homogeneous beam around the azimuth (x-y) plane. In this mode of operation, the antenna resembles an Alford Loop Design [15], [16] but with square-shaped branches. The uniform current distribution is responsible for generating the omnidirectional radiation pattern, as shown in Fig. 5(a). The simulated peak gain is about 2.5 dB at the frequency of 2.45 GHz.

2) Directional Modes: Directional beams can be excited when a single pair or metallic elements is connected to the feed port. The three disconnected pairs reflect the beam toward the excited pair and enhance its directivity. Simulations have shown that the contribution of these disconnected pairs is twofold.

To give an example, assume the scenario where the active pair is the one in positive x direction, as depicted in Fig. 5(b). Among the disconnected elements, the contribution of the only parallel pair (located in $-x$ direction) is to compress the beam along the x-axis, generating two peaks toward the end-fire directions ($\pm z$). On the other hand, a major contribution to a clear directionality is given by the two parallel pairs (located in $+y$ and $-y$ directions). The effect they provide on the directivity is for a broadside radiation directed normal to the excited pair. The additional microstrip parasitics in front of each pair of elements enhance the beam on the broadside direction increasing the gain of about 0.5 dB.

As a result of these contributions, the directional beam at 2.45 GHz shows a gain of 3.9 dB. The half-power-beamwidth, which describes the 3 dB peak extension of a directional beam, is about 60°. The four pairs of identical elements allow for the generation of a total of four distinct directional patterns spaced 90° between each other.

Once the antenna was properly tuned for the desired impedance matching and radiation patterns, a first prototype was manufactured through a milling machine process. The board was then populated with the SMD components constituting the optical switching circuitry, as shown in Fig. 4. The next two sections describe the antenna's performance in terms of input impedance and radiation pattern, compared to standard electrical control.

B. Input Impedance

The return loss is defined as the ratio between the power reflected back from the antenna port and the power delivered. It is determined by the scattering parameter S_{11}, which describes the impedance matching between a 50 Ω line and the antenna port. In our case, the antenna design was tuned to exhibit good impedance matching within the WiFi band from 2.41 to 2.48 GHz in all the configurations. Good impedance matching is assumed when $S_{11} \leq -10$ dB, as it means that more than 90% of the input RF energy is actually fed to the antenna.

The measurements were conducted by first calibrating an Agilent N5230A vector network analyzer. Next, the optical power was equally split to illuminate all the four phototransistors, provided by the same VCSEL 850 nm laser used for the measurements described in Section II-B. The power was split by means of a 1×4 fiber optic coupler with 3 dB insertion loss and plastic housing of precise alignment at the fiber optics terminations. The VCSEL laser source was tuned for equal 20 mW in each output and the correct p-i-n diode insertion loss verified through the S-parameter fixture of Fig. 2(a).

For performance comparison, we manufactured an electrically controlled version of the same antenna. Four copper wires were soldered on the RF-chokes for driving the p-i-n diodes through external dc power supply. By looking at the return loss of both omnidirectional and directional states, depicted in Fig. 6(a) and (b), respectively, it can be seen that the S_{11} resonance peaks are in good agreement between measurements and simulations. In Table III, we summarize the simulated 10 dB bandwidth for each state, along with comparison between electrical and optical

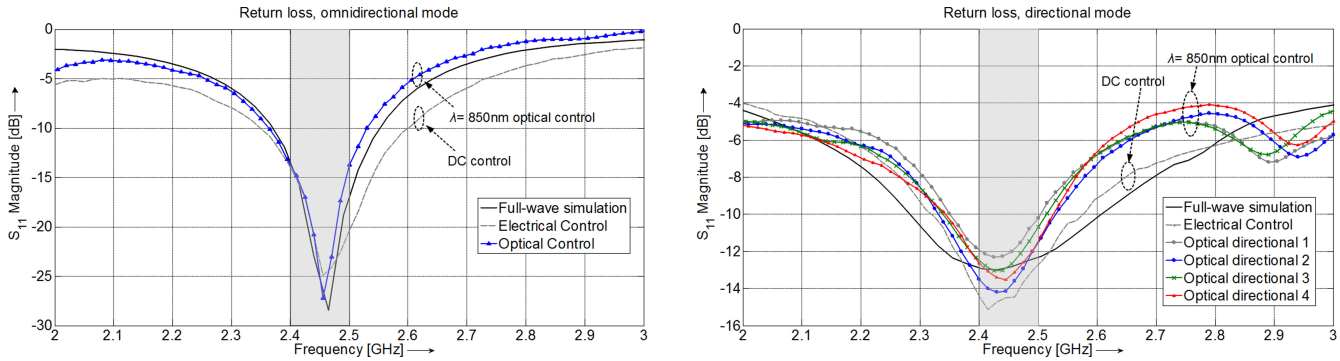

Fig. 6. Simulated return loss for each antenna state and comparison of measurements between electrical and optical control. (a) Omnidirectional mode (b) Directional mode. While the simulated S_{11} is always identical for each directional state, some slight differences occur in real scenario when the four directional modes are measured under light illumination.

TABLE III
BANDWIDTH COMPARISON BETWEEN OPTICAL CONTROL, ELECTRICAL CONTROL AND SIMULATION

Control	Omnidirectional BW	ΔBW	Directional BW	ΔBW
Optical	160 MHz	-	200 MHz*	-
Electrical	250 MHz	90 MHz	250 MHz	50 MHz
Simulation	150 MHz	10 MHz	330 MHz	130 MHz

* Average of the four curves

controls. It can be noted that the measured bandwidths under optical control are slightly less than the simulations and dc control, although maintaining good impedance matching from 2.45 to 2.48 GHz.

While moderate shifts in frequency and absolute peak amplitudes are commonly due to manufacturing tolerances and manual population of the board, the smaller bandwidth exhibited by the optical control is potentially due to the reactive lumped elements as part of the control circuitry. Nonetheless, even with this bandwidth reduction, the manufactured antenna covers the entire 2.4 GHz band with good impedance matching in all the configurations under optical control.

C. Radiation Patterns

The radiation patterns characterize the variation of the far-field radiation magnitude as a function of angular steps at a specific frequency. In order to evaluate the radiation characteristics of the proposed antenna, we have measured the radiation patterns in the case of single omnidirectional mode and for all the four directional beams. For this purpose, instead of using a conventional anechoic chamber, we have used the tool EMSCAN RFxpert [26] which is highly convenient when measuring optically-controlled antennas. This tool is a bench-top measurement system that enables us to get 3D and 2D antenna pattern measurements in real time, avoiding the need of cumbersome arrangements of cables and fiber optics around the turntable of an anechoic chamber.

Fig. 7(a) and (b) show measurements of the omnidirectional and directional mode. Each figure shows azimuth $(x-y)$ and elevation $(x-z)$ cuts of the pattern, according to the antenna coordinate system given in the insets. When all the four phototransistors are illuminated, the four microstrip elements pairs are connected to the central feed port and the excited uniform current distribution generates an omnidirectional mode illustrated in Fig. 7(a). The results show a peak gain of about 2 dBi and uniform omnidirectional shape around the azimuth plane.

On the other hand, when just a single phototransistor is illuminated, the single pair of elements that is connected to the feed port generates a directional beam directed broadside to the active elements. As shown in Fig. 7(b), the resulting beam exhibits peak gain of 3.6 dBi and a front-to-back ratio of about 8 dB. The half-power-beamwidth is approximately 65°. In Fig. 7(c) we show the azimuth view of all four directional beams, where it is important to recall that only one beam at time can be activated.

To further assess the radiation performance of the optical control, an electrically controlled version of the same antenna was also measured and compared. Fig. 8 shows the measured radiation patterns of both omnidirectional and directional states. The two plots show azimuth cut, as it represents the actual beam steering plane, which also showed a more significant variation between the two control strategies. For the case of the omnidirectional state depicted in Fig. 8(a), we can note the curve relative to the electrical control is less uniform than the optical control. Specifically, around the regions where the four metallic wires were connected, the radiation pattern exhibits a gain reduction between 2 dB $\leq \Delta G \leq$ 3 dB. Despite the envelope resemblance to an omnidirectional beam, the presence of wires interfere with the radiated field causing local magnitude reductions in the order of 40–50%. For the second case relative to directional state in Fig. 8(b), the peaks of broadside magnitude between the two curves are quite similar. The presence of wires enlarges the back lobes, reducing the front-to-back ratio. Even by looking at other existing solutions, we can see that the presence of metallic wires is a factor that reduces the homogeneity of omnidirectional radiation patterns [17], [18]. This challenge is amplified especially when the dc wires are soldered in locations corresponding to higher radiation intensity.

Moreover, it is important to highlight how the proposed antenna topology enables a fully optical control of the p-i-n diodes.

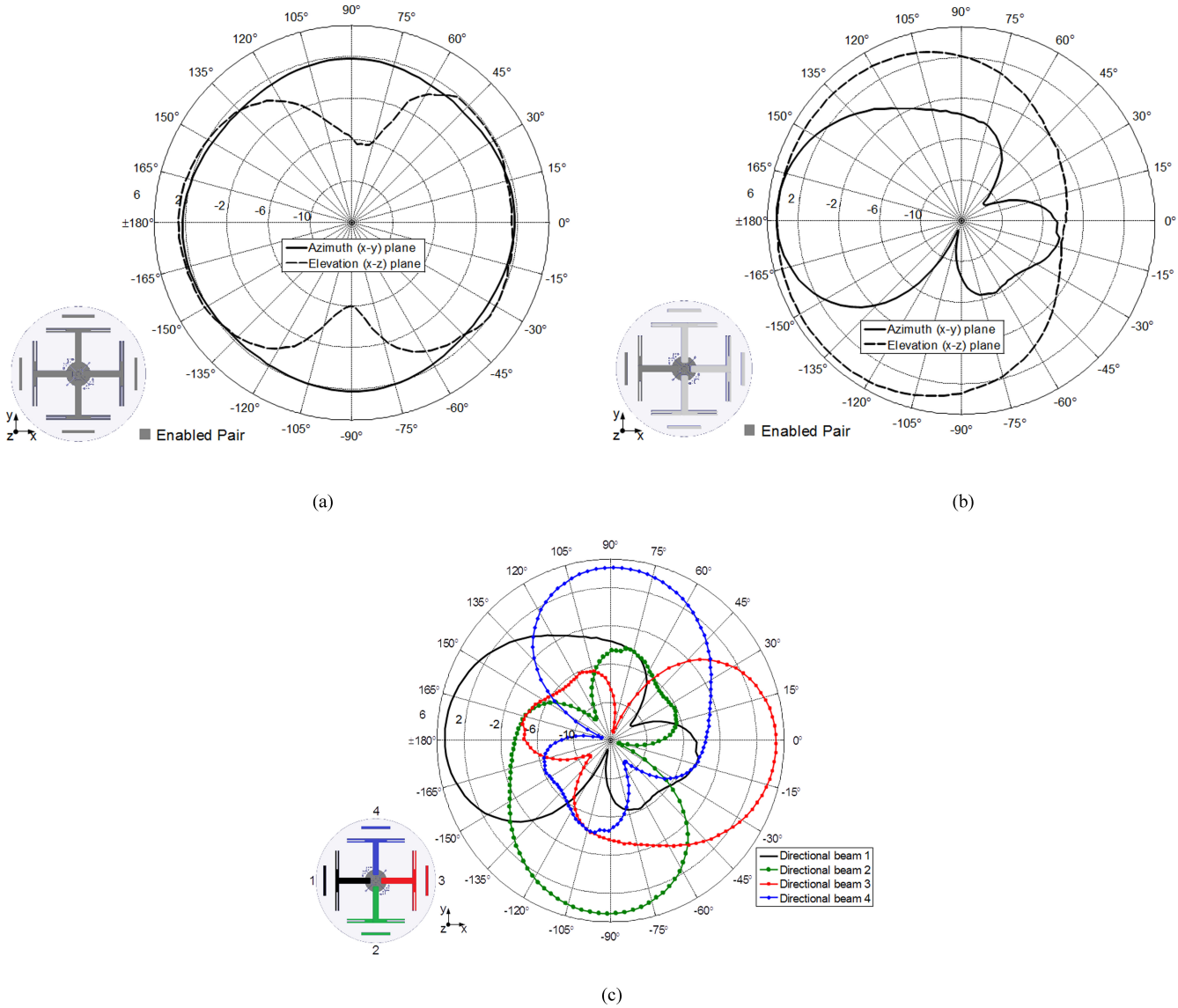

Fig. 7. Measured radiation patterns, at 2.45 GHz. (a) Omnidirectional beam, azimuth and elevation view. All the microstrip elements are connected to the central port. (b) Single directional beam, azimuth and elevation view. In this example, only the pair of elements along negative x axis is activated. (c) Azimuth view summary of the four possible directional beams. Note that each beam is activated singularly.

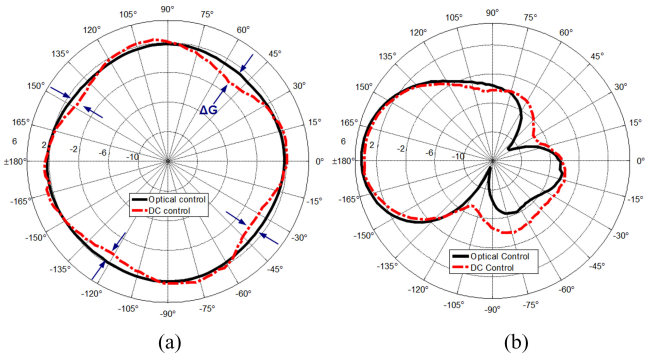

Fig. 8. Comparison of radiation patterns between optical and electrical control of the proposed reconfigurable antenna. (a) Omnidirectional state. (b) Directional state. Measurements conducted at 2.45 GHz.

In fact, the layout allows for extraction of the dc current from the coaxial RF port, eliminating not only the switching control wires, but also the dc feed lines. This key feature allows for a fully optical control, which could not be realized with concurrent planar antennas that achieve similar patterns reconfigurability [19].

D. Pattern Diversity Analysis for Multiple-Input-Multiple-Output (MIMO) Applications

Radiation pattern diversity in wireless communications is recognized as a key parameter to improve spectrum efficiency and capacity [10]. Since the antenna has been designed for application in MIMO WLAN systems, in this section we assess the performance in terms of pattern diversity. We assume a realis-

TABLE IV
MAXIMUM SPATIAL CORRELATION AND MUTUAL COUPLING BETWEEN PATTERNS USING TWO ANTENNAS

Antennas state	ρ	Coupling
Omni - Omni	0.003	-22 dB
Max {Omni, Dir}	0.005	-18 dB
Max {Dir, Dir}	0.003	-16 dB

tic scenario where two of these antennas are employed as part of a 2×2 MIMO access point. Two antennas under the same optical setup as in Section III-B, were aligned at a distance of $\lambda/4 = 31$ mm and connected to a vector network analyzer. The antenna diversity was computed from the following equation for the spatial correlation coefficient [20], expressed in terms of the S-parameters measured at 2.45 GHz:

$$\rho = \frac{\left|S_{11}^{*}S_{12} + S_{21}^{*}S_{22}\right|^{2}}{(1 - ((|S_{11}|^{2} + |S_{21}|^{2}))(1 - (|S_{22}|^{2} + |S_{12}|^{2}))}. \quad (1)$$

Since each antenna can generate 5 different radiation patterns, the total number of radiation pairs in a 2×2 array is 25, where half of the amount contains symmetrical permutations. For brevity, Table IV shows the maximum spatial correlation for the three significant subsets of states, along with the respective maximum coupling between the two radiators.

Overall, the measurements show low levels of patterns correlation, denoting a high spatial diversity. The 4G standard set $\rho = 0.3$ as maximum correlation coefficient, while the maximum measured correlation is $\rho = 0.005$. In terms of mutual coupling between the two radiators, the maximum coupling is $S_{21} = S_{12} = -16$ dB when both antennas are in directional state. However, the majority of the remaining states exhibit couplings below -30 dB. These coupling regimes indicate sufficient isolation between two antennas to be used as a two-element array in a MIMO system.

Since the antenna has high potential to be used as part of a MIMO system, concerns may arise in terms of the p-i-n diodes non-linearity. In order to address this consideration, in a previous work [21] we have demonstrated that when two antennas of a similar type are employed in a 2×2 MIMO system, the influence of intermodulation distortions (IMD) are relatively low. The third-order IMDs are on the order of –100 dBm, approaching the typical OFDM noise floor of -110 dBm.

IV. CONCLUSION

In this paper we evaluated two possible optical strategies to switch microstrip elements on reconfigurable antennas. We have focused on two commercially available devices and qualitatively analyzed their respective performances in terms of isolation and insertion loss.

The first method employs a p-i-n photodetector equipped with fiber optic, for convenient optical control. Despite the success of enhancing the change of its intrinsic capacitance, the device exhibits good insertion loss but poor isolation to be employed as SPST RF switch. Through extended numerical simulations, it was identified the optimal capacitance range to successfully employ a p-i-n photodetector as RF switching device within the 2.4 GHz WiFi band.

Consequently, we have investigated an alternative method which combines an RF p-i-n diode activated by a phototransistor. The measured scattering parameters as a function of the incident light have shown that the p-i-n diode can successfully provide appropriate values of isolation and insertion loss under light control.

This latter strategy has been applied to a novel patter-reconfigurable planar antenna, which is able to generate a single omnidirectional and four directional beams. Four phototransistors, along with proper biasing networks, have been mounted to drive the p-i-n diodes and switching between four couples of microstrip elements. Comprehensive input impedance and radiation pattern measurements have shown that the antenna performance is in good agreement with the expected behavior for all the configurations under light control. Additional comparisons with an electrically controlled prototype have shown that the optical strategy can effectively reduce the far-field interferences occurring under conventional wired dc control.

In summary, optical control of reconfigurable antennas through commercially available devices has been shown successful at a relatively low cost and moderate optical power. Addressing the technology to the next generation of cognitive radios, our next step is to employ this novel antenna with its optical control circuitry for wireless throughput measurements and Direction Of Arrival estimation.

REFERENCES

[1] A. S. Daryoush, K. Bontzos, and P. R. Herczfeld, "Optically tuned patch antenna for phased array applications," presented at the Int. Symp. Antennas Propag. Soc., Philadelphia, PA, USA, 1986.
[2] P. Qui, A. Weily, Y. Guo, T. Bird, S. Trevor, and C. Liang, "Frequency reconfigurable quasi-Yagi folded dipole antenna," *IEEE Trans. Antennas Propag.*, vol. 58, no. 8, pp. 2742–2747, Aug. 2010.
[3] Y. Zhou, R. Adve, and S. Hum, "Design and evaluation of pattern reconfigurable antennas for MIMO applications," *IEEE J. Select. Areas Commun.*, vol. 62, no. 3, pp. 1084–1092, Mar. 2014.
[4] D. Piazza, P. Mookiah, M. D'Amico, and K. R. Dandekar, "Pattern and polarization reconfigurable circular patch for MIMO systems," in *Proc. IEEE Eur. Conf. Antennas Propag.*, 2009, pp. 1047–1051.
[5] D. Patron, H. Paaso, A. Mammela, D. Piazza, and K. R. Dandekar, "Improved deisgn of a CRLH leaky-wave antenna and its application for DoA estimation," in *Proc. IEEE-APS Top. Conf. Antennas Propag. Wireless Comm.*, 2013, pp. 1343–1346.
[6] Y. Tawk, A. R. Albrecht, S. Hemmady, and G. Balakrishnan, "Optically pumped frequency reconfigurable antenna design," *IEEE Antennas Wireless Propag. Lett.*, vol. 9, pp. 280–283, Apr. 2010.
[7] Y. Tawk, S. Hemmady, C. G. Christodoulu, J. Costantine, and G. Balakrishnan, "A cognitive radio antenna design based on optically pumped reconfigurable antenna system (OPRAS)," in *Proc. IEEE Int. Symp. Antennas Propag.*, 2011, pp. 1116–1119.
[8] G. P. Jin, D. L. Zhang, and R. L. Li, "Optically controlled reconfigurable antenna for cognitive radio applications," *IET Electron. Lett.*, vol. 47, no. 17, pp. 948–950, 2011.
[9] J. P. Panagamuwa, A. Chauraya, and J. C. Vardaxoglou, "Frequency and beam reconfigurable antenna using photoconductive switches," *IEEE Trans. Antennas Propag.*, vol. 54, no. 2, pp. 449–454, Feb. 2006.
[10] D. Piazza, N. J. Kirsch, A. Forenza, R. W. Heath, and K. R. Dandekar, "Design and evaluation of a reconfigurable antenna array for MIMO systems," *IEEE Trans. Antennas Propag.*, vol. 56, no. 3, pp. 869–881, Mar. 2008.
[11] R. Ibernon-Fernandez, J. Molina-Garcia-Pardo, and L. Juan-Llacer, "Comparison between measurements and simulations of conventional and distributed MIMO system," *IEEE Antennas Wireless Propag. Lett.*, vol. 7, pp. 546–549, Aug. 2008.

[12] D. Patron, K. R. Dandekar, and A. S. Daryoush, "Optical control of pattern-reconfigurable antennas," in *Proc. IEEE Int. Top. Meeting Microw. Photon.*, 2013, pp. 33–36.
[13] F. Capasso, R. A. Logan, and W. T. Tsang, "Interdigitated pn junction device with novel capacitance/voltage characteristic, ultralow capacitance and low punch/through voltage," *Electron. Lett.*, vol. 18, no. 18, pp. 760–761, 1982.
[14] X. Zhao, A. Cola, A. Tersigni, F. Quaranta, E. Gallo, J. Spanier, and B. Nabet, "Optically modulated high-sensitivity heterostructure varactor," *IEEE Electron Device Lett.*, vol. 27, no. 9, pp. 710–712, Sep. 2006.
[15] A. Alford and A. G. Kandoian, "Ultra-high frequency loop antenna," *Trans. AIEE*, vol. 59, pp. 843–848, 1940.
[16] C. H. Ahn, S. W. Oh, and K. Chang, "A dual-frequency omnidirectional antenna for polarization diversity of MIMO and wireless communication applications," *IEEE Antennas Wireless Propag. Lett.*, vol. 8, pp. 966–969, Aug. 2009.
[17] W. S. Kang, J. A. Park, and Y. J. Yoon, "Simple reconfigurable antenna with radiation pattern," *Electron. Lett.*, vol. 44, no. 3, pp. 182–183, 2008.
[18] T. Abouful, A. Alomainy, and C. Parini, "Reconfiguring UWB monopole antenna for cognitive radio applications using GaAs FET switches," *IEEE Antennas Wireless Propag. Lett.*, vol. 11, pp. 392–394, Apr. 2012.
[19] M. Facco and D. Piazza, "Reconfigurable zero-order loop antenna," in *Proc. IEEE Antennas Propag. Soc. Int. Symp.*, 2012, pp. 1–2.
[20] S. Blanch, J. Romeu, and I. Corbella, "Exact representation of antenna system diversity performance from input parameter description," *Electron. Lett.*, vol. 39, no. 9, pp. 705–707, 2003.
[21] D. Patron, A. S. Daryoush, D. Piazza, and K. R. Dandekar, "Design and harmonic balance analysis of a wideband planar reconfigurable antenna having omnidirectional and directional patterns," in *Proc. IEEE 14th Annu. Wireless Microw. Tech. Conf.*, 2013, pp. 1–5.
[22] Everlight PT19-21B *Technical Data Sheet.* (2013). [Online]. Available: http://www.everlight.com/datasheets/PT19–21B-L41-TR8_datasheet.pdf
[23] Fermionics FD-80 PIN Photodiode *Technical Data Sheet* . [Online]. Available: http://www.fermionics.com/PDF%20files/FD80%20series.pdf
[24] *Ansoft HFSS User Manual*, Ansoft Corp., Pittsburg, PA, USA, 2005.
[25] Skyworks SMP-1345 *Technical Data Sheet*. (2012). [Online]. Available: http://www.skyworksinc.com/uploads/documents/200046M.pdf
[26] *RFxpert User Manual*. EMSCAM. (2013). [Online] Available: http://www.emscan.com/downloads/RFxpert/Technical_Resources/RFxpert_User_Manual_v2.1.pdf

Damiano Patron (S'11) received the B.S. degree in electronics engineering from the University of Padua, Padua, Italy, in 2010, and the M.S. degree in electrical and computer engineering from Drexel University, Philadelphia, PA, USA, in 2013, where he is currently working toward the Ph.D. degree in telecommunication engineering.

From 2002 to 2010, he worked with Euro-Link S.r.l. as a System Integrator of RFID systems. In 2010, he joined the start-up company Adant Inc. as an RF and Antenna Engineer, designing reconfigurable antennas for WiFi and RFID applications. His research interests include the design of reconfigurable antennas for throughput maximization and DoA estimation in wireless networks. He also works in the development of wearable sensors and power harvesting systems. He is the author and coauthor of several patents in the field of reconfigurable antennas, antennas miniaturization, and wearable technologies.

Patron received several awards including the Drexel Frank and Agnes Seaman Fellowship Award in 2013 and the Young Scientist Best Paper Award at the ICEAA–IEEE APWC–EMS 2013 Conference.

Afshin S. Daryoush (S'84–M'86–SM'90–F'99) received the Ph.D. degree in electrical engineering from Drexel University, Philadelphia, PA, USA, in 1986.

He has been a Full Professor at Drexel University since 1998. As part of the Sabbatical Leave Awards from Drexel University, he worked as a Visiting Scholar at NTT Wireless Systems Laboratories, Yokosuka, Japan (1996–1997) and at the CNRS' Institute of Electronics, Microelectronics, and Nanotechnologies, Villeneuve d'Asq., Lille, France (2005); since then, he also collaborated with researchers at Thales LRC, Orsay, France; Alcatel Thales III–V Lab, Marcoussie, France; and faculty members from the University of Rennes and University of Nantes in France.

Dr. Daryoush received the Drexel University Graduate Teaching Award in 2000 and he has developed and taught a variety of undergraduate and graduate courses in electromagnetic fields, telecommunication, wireless communications, solid-state microwave and photonic devices, RF circuits, and antennas. He has also conducted research in microwave photonics for wireless communication, satellite communications, EW, and biomedical engineering applications, resulting in publication of more than 200 technical papers and seven book chapters. He has also delivered invited talks on biomedical, telecommunications, and military systems employing various Microwave Photonics techniques in many symposia, the U.S. Government and NATO sponsored workshops, and international research laboratories. He received seven U.S. patents and two additional ones pending. He has been a Member of Sigma Xi since 1986 and has served as the President of the Drexel University Chapter in 1999. He has also served as the Chair of the IEEE Philadelphia Joint Chapter of the AP/MTT Societies (1991–1993 and 2013–2014). He serves as the Faculty Advisor to the Graduate Student Chapter of IEEE at Drexel University since 1998. He had (co)organized and served as General Steering Committee Chair or TPC Chair of the Benjamin Franklin Symposium (1989–1996 and BenMAS2014), the IEEE Microwave Photonics (MWP'98, MWP'10, MWP'12, and MWP'14), the International Microwave Symposium (IMS'03 and IMS'08), the IEEE Radio Wireless Symposia (RWS'08 and RWS'09), the IASTED's Antenna, Radar, and Wave Propagation Conference (ARP'08). He has served as a Guest Editor for the IEEE TRANSACTIONS ON MICROWAVE THEORY AND TECHNIQUES, *The Journal of the Franklin Institute*, and *Microwave & Lightwave Technology Letters*.

Kapil R. Dandekar (S'95–M'01–SM'07) received the B.S. degree in electrical engineering from the University of Virginia, Charlottesville, VA, USA, in 1997. He received the M.S. and Ph.D. degrees in electrical and computer engineering from the University of Texas at Austin, Austin, TX, USA, in 1998 and 2001, respectively.

In 1992, he worked at the U.S. Naval Observatory, and from 1993 to 1997, he worked at the U.S. Naval Research Laboratory. In 2001, he joined the Department of Electrical and Computer Engineering, Drexel University in Philadelphia, Philadelphia, PA, USA. He is currently a Professor in the Department of Electrical and Computer Engineering, Drexel University; the Director of the Drexel Wireless Systems Laboratory (DWSL); an Associate Dean for Research in the Drexel University College of Engineering. DWSL has been supported by the U.S. National Science Foundation, Army CERDEC, National Security Agency, Office of Naval Research, and private industry. His current research interests and publications include wireless, ultrasonic, and optical communications, reconfigurable antennas, and smart textiles. Intellectual property from DWSL has been licensed by external companies for commercialization. He is also a past and current Member of the IEEE Educational Activities Board and Cofounder of the EPICS-in-IEEE program.